Journal of Power Sources 195 (2010) 6867–6872

Contents lists available at ScienceDirect

Journal of Power Sources

journal homepage: www.elsevier.com/locate/jpowsour

Electrochemical and structural studies of $LiCo_{1/3}Mn_{1/3}Fe_{1/3}PO_4$ as a cathode material for lithium ion batteries

Yi-Chun Chen [a], Jin-Ming Chen [b], Chia-Haw Hsu [b], Jey-Jau Lee [c], Tsung-Chi Lin [d], Jien-Wei Yeh [a], Han C. Shih [a,d,*]

[a] Department of Materials Science and Engineering, National Tsing Hua University, Hsinchu 300, Taiwan
[b] Materials and Chemical Engineering, Industrial Technology Research Institute, Chutung 310, Taiwan
[c] National Synchrotron Radiation Research Center, Hsinchu 300, Taiwan
[d] Institute of Materials Science and Nanotechnology, Chinese Culture University, Taipei 111, Taiwan

ARTICLE INFO

Article history:
Received 19 November 2009
Received in revised form 25 January 2010
Accepted 25 January 2010
Available online 2 February 2010

Keywords:
Olivine structure
Synchrotron X-ray
diffusivity
Lithium multi-transition metal phosphate

ABSTRACT

A solid-state reaction to synthesize a lithium multi-transition metal phosphate $LiCo_{1/3}Mn_{1/3}Fe_{1/3}PO_4$ is used in this work, which has a high voltage of 3.72 V and capacity of 140 mAh g^{-1} at a 0.05 C rate. From the in-situ XRD analysis, $LiCo_{1/3}Mn_{1/3}Fe_{1/3}PO_4$ has shown a high stability during cell charge/discharge, even operating at 5 V, which is due to the stable olivine structure. Although all the transition metals Co^{2+}, Mn^{2+} and Fe^{2+} are at the same 4c site of the $LiCo_{1/3}Mn_{1/3}Fe_{1/3}PO_4$ structure, they seem to have different chemical activities and reflect on the electrochemical performance. The capacity contributed by the Co^{2+}/Co^{3+} redox couple is only 20 mAh g^{-1}, which is less than that of the Fe^{2+}/Fe^{3+} and Mn^{2+}/Mn^{3+} redox couples. This is because of the fact that the diffusivity of lithium ion for the Co^{2+}/Co^{3+} redox couple is 10^{-16} cm^2 s^{-1} which is one order less than that of the Fe^{2+}/Fe^{3+} and Mn^{2+}/Mn^{3+} redox couples in $LiCo_{1/3}Mn_{1/3}Fe_{1/3}PO_4$.

1. Introduction

Since the olivine structure of $LiFePO_4$ was reported by Goodenough and co-workers [1], it has attracted greatly attention due to its low cost and the safety issue [2–4]. However its low electrical conductivity and working voltage impose a limitation on its applications for commercial products. In order to solve these problems, much effort has been made by several research groups. For example, electrical contact to $LiFePO_4$ can be improved by the carbon coatings [5–8], and the intrinsic electronic conductivity can be increased by the super-valence ion doping of the Li-site, and the mean free path is decreased by reducing the particle size [9–11].

Recently, the focus of research has been changed to other olivine-type cathode materials such as $LiMnPO_4$, $LiCoPO_4$ and $LiNiPO_4$ because the chemical potentials of Mn^{2+}/Mn^{3+}, Co^{2+}/Co^{3+} and Ni^{2+}/Ni^{3+} are higher than that of the Fe^{2+}/Fe^{3+} couple at 4.1, 4.8 and 5.1 V [12], respectively. However, the compounds of $LiMPO_4$ (M = Mn, Co and Ni) do not exhibit good electrochemical performance because of the lower electrical conductivity compared to $LiFePO_4$. In order to improve the electrical conductivity and consequent performance, solid solutions of lithium multi-transition-metal phosphates have been prepared, including $LiMn_xFe_{1-x}PO_4$ reported by Yamada' group [13]. Moreover, Kuo et al. substituted Mn by Co to reduce the effect of Jahn–Teller distortion of Mn^{3+} so that $LiMn_{0.35}Co_{0.2}Fe_{0.45}PO_4$ was successfully synthesized [14]. In order to investigate the lithium diffusivity of lithium multi-metal phosphate, $LiCo_{1/3}Mn_{1/3}Fe_{1/3}PO_4$ was synthesized and ex-situ electrochemical impedance spectroscopy experiment was employed to investigate the lithium diffusivity of each phase transition reaction from M^{2+} to M^{3+}. Ni was not taken into consideration because the chemical potential of the Ni^{2+}/Ni^{3+} couple is too high (5.1 V) and the electrolyte is unable to cope with such high potential. Based on the previous report [15,16], $LiNiPO_4$ also showed very poor electrochemical performance. Even forming part of the solid solution $LiFe_{1/4}Mn_{1/4}Co_{1/4}Ni_{1/4}PO_4$, the Ni^{2+}/Ni^{3+} redox couple did not work.

2. Experimental

2.1. Powder preparation and cell fabrication

The compound $LiCo_{1/3}Mn_{1/3}Fe_{1/3}PO_4$ was prepared by solid-state reaction between the compounds $FeC_2O_4{\cdot}2H_2O$, $MnCO_3$, $NH_4H_2PO_4$, $Co(NO_3)_2{\cdot}6H_2O$ and Li_2CO_3 in stoichiometric amounts. Some glucose was added in order to enhance the conductivity and prevent the formation of Fe^{3+}, Mn^{3+} and Co^{3+}. The precursors were

* Corresponding author at: Department of Materials Science and Engineering, National Tsing Hua University, Hsinchu 300, Taiwan. Tel.: +886 3 5715131 3845; fax: +886 3 5710290.
E-mail address: hcshih@mx.nthu.edu.tw (H.C. Shih).

0378-7753/$ – see front matter.
doi:10.1016/j.jpowsour.2010.01.058

dispersed in ethanol and ground by ball-milling. After evaporating the ethanol, the mixtures were first heated at 350 °C for 10 h in N_2 ambient. The resulting $LiCo_{1/3}Mn_{1/3}Fe_{1/3}PO_4$ was subsequently sintered at 550 °C in N_2 ambient for 30 h.

The cathode was constructed from $LiCo_{1/3}Mn_{1/3}Fe_{1/3}PO_4$/carbonblack/polyvinylidene fluoride, with a weight ratio of 85/8/7, on an aluminum film. The electrochemical performance was measured using a coin cell 2032, which was assembled as follows: cathode, anode (lithium metal) and electrolyte (1 M $LiPF_6$ in an ethylene carbonate (EC) and dimethyl carbonate (DMC) mixed solvent with a volume ratio of 1:1.)

2.2. Electrochemical tests and characterization of materials

The cells were charged and discharged at 25 °C between fixed voltage limits (5–2 V) on an Arbin BT2400 battery tester. The cyclic voltammetry and electrochemical impedance spectroscopy (EIS) were measured by an Autolab PGSTAT30. The sinusoidal excitation voltage applied to the cells was 10 mV at different frequencies ranging from 100 kHz to 10 mHz. The EIS data was fitting by ZView (version 2.6b).

The structures were determined by synchrotron X-ray diffraction, carried out in transmission mode at 9.3 keV (λ = 1.3362 Å) at the Wiggler beam line 17A of the National Synchrotron Radiation Research Center, Hsinchu, Taiwan. The exposure time was 30 s and the XRD spectra were recorded on the Mar 345-image plate detector. Before further analysis, all in-situ XRD patterns were calibrated using standard samples (Ag + Si). The morphology of the $LiCo_{1/3}Mn_{1/3}Fe_{1/3}PO_4$ powder is studied by scanning electron microscopy (High Resolution Hyper Probe JXA-8500F).

3. Results and discussion

3.1. Structure and morphology analysis

In order to obtain a high resolution to analyze materials, synchrotron X-ray is used because of its high energy, continuous spectrum, excellent collimation and low emittance. Recently, the synchrotron X-ray analysis has been widely employed to study the lithium ion batteries [17–21]. Fig. 1 and Table 1 show Rietveld refinement results of the $LiCo_{1/3}Mn_{1/3}Fe_{1/3}PO_4$ powder. There are no impurities observed in the XRD pattern and all the peaks indicated for $LiCo_{1/3}Mn_{1/3}Fe_{1/3}PO_4$ belong to an olivine structure (Pnma). There are also no peak separation as shown in Fig. 1, suggesting that $LiCo_{1/3}Mn_{1/3}Fe_{1/3}PO_4$ is a solid solution of $LiFePO_4$, $LiMnPO_4$ and $LiCoPO_4$. The lattice parameters are calculated by General Structure Analysis System (GSAS) software: a = 10.329 Å, b = 6.017 Å and c = 4.711 Å. The lattice parameters are in good agreement with Chen et al. [22], a = 10.338 Å, b = 6.009 Å and c = 4.718 Å. Fig. 2 shows the morphology of the $LiCo_{1/3}Mn_{1/3}Fe_{1/3}PO_4$ powder. The particle size is about 10 μm and in a spherical shape.

3.2. Electrochemical performances

Fig. 3 shows the electrochemical performance of $LiCo_{1/3}Mn_{1/3}Fe_{1/3}PO_4$ at different discharge rates. There are three distinct voltage plateaux, at 3.5, 4.1 and 4.7 V, which correspond to the Fe^{2+}/Fe^{3+}, Mn^{2+}/Mn^{3+} and Co^{2+}/Co^{3+} redox couples, respectively. At a 0.05 C charge/discharge rate, the reversible capacity is about 140 mAh g^{-1} and the average voltage also rises to 3.72 V due to the incorporation of Mn and Co. However, $LiCo_{1/3}Mn_{1/3}Fe_{1/3}PO_4$ does not show good electrochemical performance at higher charge/discharge rates. The capacity and voltage decrease with increasing discharge rate due to its poor electrochemical properties. Although $LiCo_{1/3}Mn_{1/3}Fe_{1/3}PO_4$ is a solution of $LiFePO_4$, $LiMnPO_4$ and $LiCoPO_4$, the Co^{2+}/Co^{3+} redox couple seems to have less activity than the Fe^{2+}/Fe^{3+} and Mn^{2+}/Mn^{3+} redox couples. At a 0.05 C discharge rate, the reversible capacity contributed by

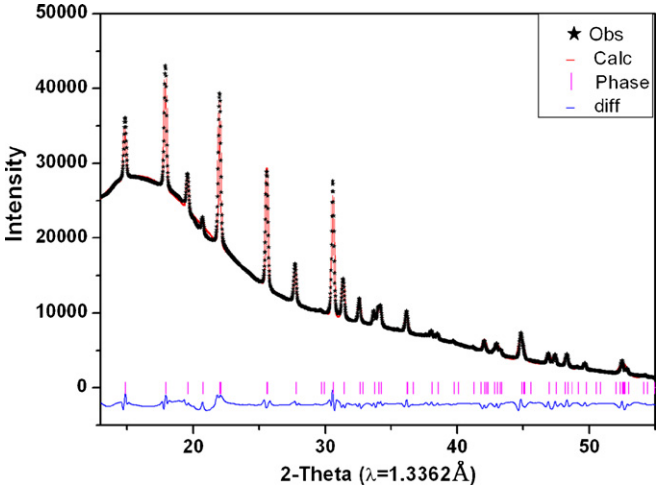

Fig. 1. Rietveld refinement pattern of the synchrotron X-ray data for the $LiCo_{1/3}Mn_{1/3}Fe_{1/3}PO_4$ powder.

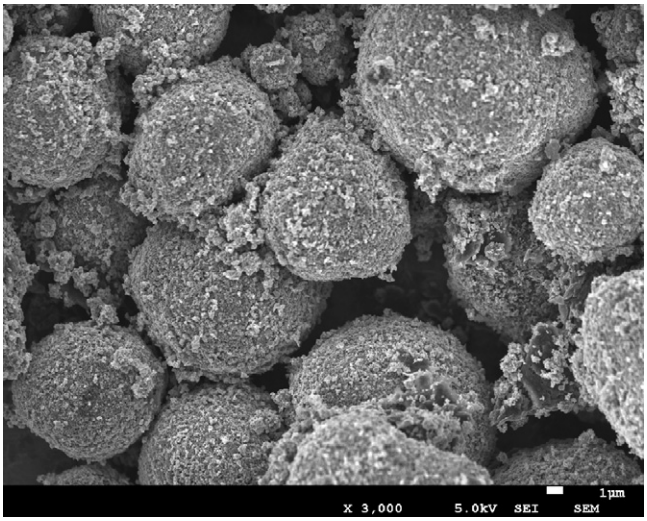

Fig. 2. SEM image of the $LiCo_{1/3}Mn_{1/3}Fe_{1/3}PO_4$ powder.

Table 1
Rietveld refinement results for the $LiCo_{1/3}Mn_{1/3}Fe_{1/3}PO_4$ powder with synchrotron X-ray diffraction data.

Atom	Site	g	x	y	z	Uiso
Li	4a	1	0	0	0	0.0972 (8)
Co, Mn, Fe	4c	1	0.2817 (4)	0.25	0.9725 (3)	0.0525 (9)
P	4c	1	0.0947 (6)	0.25	0.4334 (5)	0.0619 (9)
O_1	4c	1	0.1022 (3)	0.25	0.7516 (6)	0.0645 (7)
O_2	4c	1	0.4684 (0)	0.25	0.1750 (0)	0.0486 (4)
O_3	8d	1	0.1674 (6)	0.0511(5)	0.2850 (9)	0.0460 (9)

Fitted R_{wp} = 2.51% and R_p = 1.54%; Bknd R_{wp} = 5.52% and R_p = 3.06%; reduced CHI**2 = 7.625.

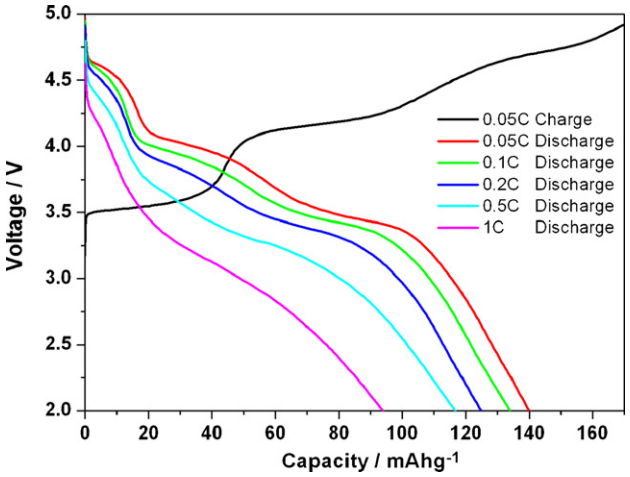

Fig. 3. Electrochemical performances of the $LiCo_{1/3}Mn_{1/3}Fe_{1/3}PO_4$ cathode at various discharge rates.

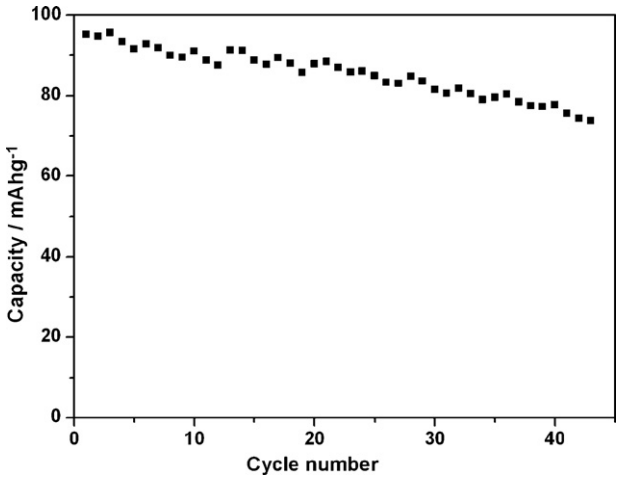

Fig. 4. Cyclic performances of the $LiCo_{1/3}Mn_{1/3}Fe_{1/3}PO_4$ cathode at 0.2 C charge/discharge rate.

the Co^{2+}/Co^{3+} redox couple is only 20 mAh g^{-1}, which is much less than the theoretical specific capacity (56 mAh g^{-1}). The cyclic performance of $LiCo_{1/3}Mn_{1/3}Fe_{1/3}PO_4$ is shown in Fig. 4. The cell was charged/discharged at a 0.2 C rate. The initial capacity is only 95 mAh g^{-1} and decreased with the increase of the cycle number. However, these results are not in our expectation; the olivine-type

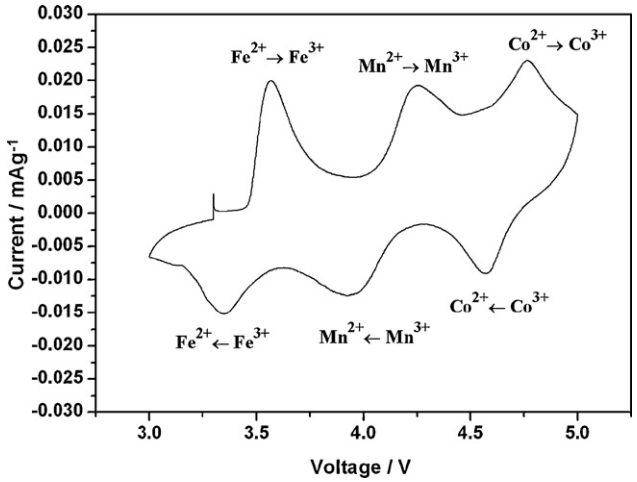

Fig. 5. Cyclic voltammetry of the $LiCo_{1/3}Mn_{1/3}Fe_{1/3}PO_4$ cathode. (scan rate = 0.05 mV s^{-1}).

$LiCo_{1/3}Mn_{1/3}Fe_{1/3}PO_4$ does not show the excellent retention of $LiFePO_4$. There are two possible reasons for this: the structure cannot sustain such high operating voltage or the electrolyte has been oxidized. Therefore an in-situ synchrotron XRD experiment was used to observe any structural change of the $LiCo_{1/3}Mn_{1/3}Fe_{1/3}PO_4$ during the cell charge/discharge. This will be discussed in a later section.

3.3. Cyclic voltammetry

The cyclic voltammogram of $LiCo_{1/3}Mn_{1/3}Fe_{1/3}PO_4$ is shown in Fig. 5. There are three obvious redox reactions at 3.45, 4.09 and 4.66 V, corresponding to the Fe^{2+}/Fe^{3+}, Mn^{2+}/Mn^{3+} and Co^{2+}/Co^{3+} redox couples, respectively. These results correlate with the three distinct plateaus in the charge/discharge curve, as shown in Fig. 3. However, the oxidation and reduction peaks of the three redox couples are not symmetric, indicating that $LiCo_{1/3}Mn_{1/3}Fe_{1/3}PO_4$ does not have good reversibility. Electrolyte oxidation is also observed in the CV curve as the voltage rises above 4.5 V, which may cause the asymmetry of the redox peaks and the poor retention of $LiCo_{1/3}Mn_{1/3}Fe_{1/3}PO_4$.

3.4. In-situ XRD analysis

Fig. 6(a) and (b) shows the in-situ synchrotron XRD analysis of the $Li_xCo_{1/3}Mn_{1/3}Fe_{1/3}PO_4$ at 0.05 C charge/discharge as

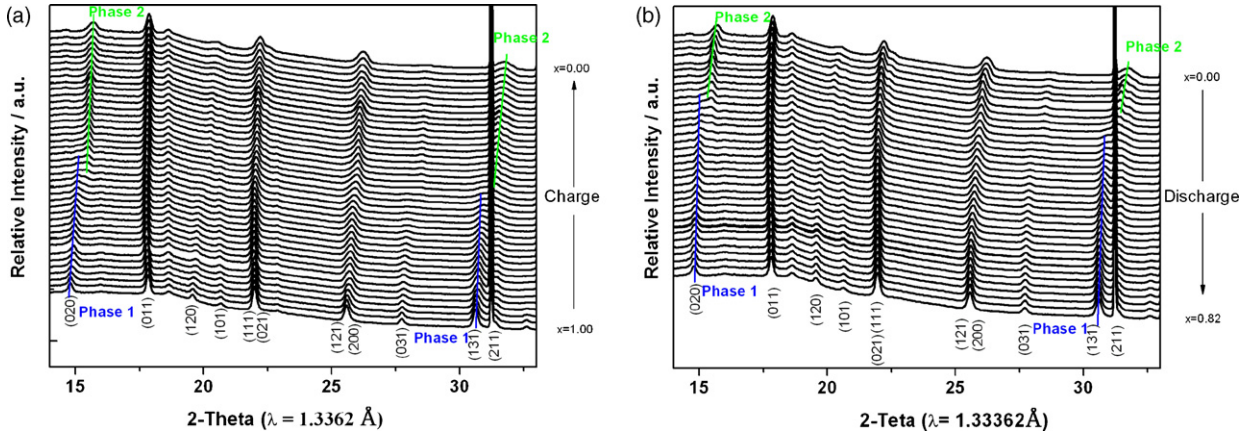

Fig. 6. In-situ synchrotron X-ray diffraction patterns of the $Li_xCo_{1/3}Mn_{1/3}Fe_{1/3}PO_4$ cathode as a function of lithium content x at 0.05 C rate (a) charge and (b) discharge.

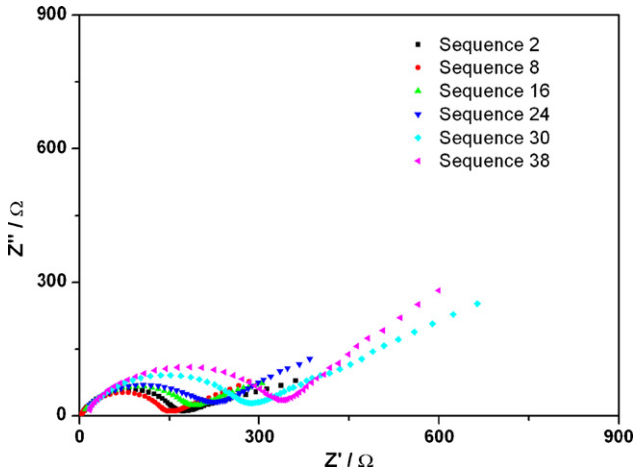

Fig. 7. EIS analysis of the $LiCo_{1/3}Mn_{1/3}Fe_{1/3}PO_4$ cathode at different charge states.

a function of the lithium content x. The first XRD pattern of $Li_xCo_{1/3}Mn_{1/3}Fe_{1/3}PO_4$ was recorded at open circuit voltage ($x = 1.00$) and measured every 30 min during the cell charge and discharge. The (0 2 0) peak reveals that $LiCo_{1/3}Mn_{1/3}Fe_{1/3}PO_4$ is the same as other olivine-type cathode materials, following the two-phase transformation during the lithium ion deintercalation and intercalation [23,24]. $LiCo_{1/3}Mn_{1/3}Fe_{1/3}PO_4$ also shows excellent electrochemical stability during the charge/discharge. This is because the presence of the polyanion $(PO_4)^{3-}$ with strong P–O covalent bonds stablilizing the metal antibonding state, which is accomplished through an M–O–P inductive effect [25]. Even when the cell is charged to 5 V, it still maintains the stable olivine structure. Therefore the fading capacity is caused by the oxidation of electrolyte during the cycling.

3.5. Ex-situ electrochemical impedance spectroscopy experiment

EIS analysis is an important technology and widely applied to the study of lithium ion batteries. The first EIS data of $LiCo_{1/3}Mn_{1/3}Fe_{1/3}PO_4$ was recorded at open circuit voltage and measured every 30 min during the cell charge. Sequence 0 was the measurement of the fresh device and sequence 1 was measured after 30 min cell charge, sequence 2 was measured after 60 min, and so on. Fig. 7 shows the EIS curve of the $LiCo_{1/3}Mn_{1/3}Fe_{1/3}PO_4$ electrode at different charge states. With the increase of the cell charge time, an obvious increase of the electrochemical resistance is obtained. An equivalent circuit as shown in Fig. 8 was used to fit these EIS data. The first resistance represents the solution resistance (R_s), parallel circuits with a resistance (R_{ct}) and a constant phase element (CPE_{ct}), which was applied to the model with the resistance of the charge-transfer reaction and double layer capacitance. At low frequency region, the Warburg impedance (Wo) is obtained (slope line) due to the mass transfer. The fitting results are shown in Table 2. In the Co^{2+}/Co^{3+} region, the $LiCo_{1/3}Mn_{1/3}Fe_{1/3}PO_4$ electrode has the highest charge-transfer resistance followed by the one in the Mn^{2+}/Mn^{3+} region. The smallest charge-transfer resistance was found in the Fe^{2+}/Fe^{3+} region. It seems that the charge-transfer resistance has a close relation to the conductivity of $LiCoPO_4$, $LiMnPO_4$ and $LiFePO_4$. Because $LiFePO_4$ has a better conductivity compared to $LiMnPO_4$ and $LiCoPO_4$ [26], the $LiCo_{1/3}Mn_{1/3}Fe_{1/3}PO_4$ electrode has the smallest charge-transfer resistance in the Fe^{2+}/Fe^{3+} region.

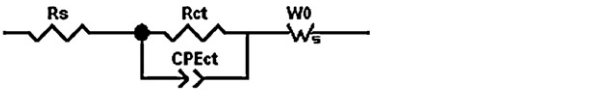

Components	Description
Rs	Solution resistance
Rct	Resistance of the charge-transfer reaction
CPEct	Double layer capacitance
Wo	Mass transfer

Fig. 8. Equivalent circuit used for fitting the experimental EIS data.

By measuring the electrochemical impedance spectrum, we obtain not only the electrochemical resistance of the material, but also the diffusivity of the lithium ions, according to the following equation [27,28]:

$$D = \frac{R^2T^2}{2n^4F^4C^2\sigma^2} \quad (1)$$

where R is the gas constant; T the absolute temperature, n is the number of electrons per molecule during the oxidization; F the Faraday constant; C the concentration of lithium ion and σ the Warburg factor which is related to Z'':

$$Z'' = \sigma\omega^{1/2} \quad (2)$$

$LiCo_{1/3}Mn_{1/3}Fe_{1/3}PO_4$ is a lithium multi-transition metal phosphate and it is very interesting to investigate the kinetics of each phase transition reaction from M^{2+} to M^{3+}. Therefore ex-situ EIS experiments were used to study the lithium diffusivity of $LiCo_{1/3}Mn_{1/3}Fe_{1/3}PO_4$. Fig. 9 shows the charge curve of the ex-situ experiment and the diffusivity of lithium ions during the cell charge. The diffusivity of lithium ions in the Fe^{2+}/Fe^{3+} and Mn^{2+}/Mn^{3+} regions is about 10^{-15} cm^2 s^{-1} whereas it is about 10^{-16} cm^2 s^{-1} in the Co^{2+}/Co^{3+} region, suggesting the reduced chemical activity of the Co^{2+}/Co^{3+} couple compared to the Fe^{2+}/Fe^{3+} and Mn^{2+}/Mn^{3+} couples in $LiCo_{1/3}Mn_{1/3}Fe_{1/3}PO_4$. This discovery explains the reason why the Co^{2+}/Co^{3+} couple has a lower reversible capacity compared to the Fe^{2+}/Fe^{3+} and Mn^{2+}/Mn^{3+} couples, as shown in Fig. 3. When the redox reaction shifts from Fe^{2+}/Fe^{3+} redox couple to Mn^{2+}/Mn^{3+} redox couple, the diffusivity falls to 10^{-17} cm^2 s^{-1}, indicating that it is very difficult for lithium ions to move in the transferring region due to the absence of the lithium ion

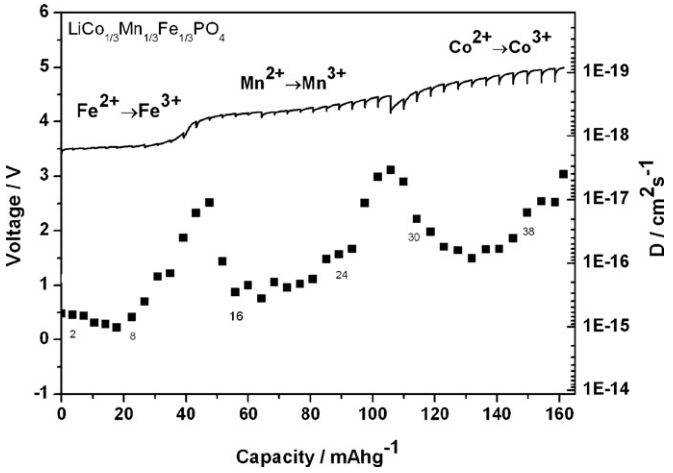

Fig. 9. Lithium diffusivities of the $Li_xCo_{1/3}Mn_{1/3}Fe_{1/3}PO_4$ cathode.

Table 2
Electrode kinetic parameters obtained from equivalent circuit fitting of experimental data for $LiCo_{1/3}Mn_{1/3}Fe_{1/3}PO_4$ during the cell charge.

Sequence	Voltage (V)	Diffusion coefficient ($cm^2\ s^{-1}$)	R_s (Ω)	CPE_{ct} (F)	CPE	R_{ct} (Ω)	Chi-squared
0	3.37	6.30E-16	3.38	9.06E-06	0.83025	270.7	0.000379
1	3.49	6.60E-16	2.69	1.19E-05	0.8	158.1	0.00525
2	3.5	6.70E-16	2.90	9.94E-06	0.82044	226.9	0.000621
3	3.51	8.70E-16	2.73	1.19E-05	0.80461	153.5	0.004237
4	3.52	9.10E-16	2.70	1.16E-05	0.8067	153	0.003125
5	3.52	1.02E-15	2.69	1.15E-05	0.80668	148.1	0.002559
6	3.54	7.03E-16	2.69	1.15E-05	0.80625	146.5	0.002682
7	3.55	4.02E-16	2.74	1.14E-05	0.8073	139	0.001884
8	3.57	1.64E-16	2.77	1.12E-05	0.80919	135.8	0.001581
9	3.63	1.45E-16	2.94	1.10E-05	0.81127	127.5	0.001316
10	3.78	4.00E-17	3.48	8.60E-06	0.82	170.4	0.001957
11	3.98	1.63E-17	4.07	7.90E-06	0.82903	141.3	0.000473
12	4.06	1.13E-17	4.50	7.54E-06	0.83725	123.7	0.001882
13	4.09	9.41E-17	3.96	7.07E-06	0.84413	133.4	0.001195
14	4.12	2.89E-16	1.92	7.45E-06	0.83004	158.9	0.000747
15	4.13	2.22E-16	4.72	7.35E-06	0.81208	259.8	0.000324
16	4.15	3.65E-16	2.41	6.98E-06	0.80195	411.4	0.000857
17	4.15	2.00E-16	1.09	8.15E-06	0.7804	252	0.002881
18	4.18	2.43E-16	32.5	2.17E-06	0.97055	191.1	0.019733
19	4.2	2.13E-16	0.99	8.10E-06	0.76126	219.5	0.000618
20	4.23	1.81E-16	0.81	8.04E-06	0.76188	203.6	0.000617
21	4.25	8.75E-17	0.11	8.01E-06	0.76023	196.8	0.00071
22	4.29	7.36E-17	0.33	7.64E-06	0.7663	184.3	0.000737
23	4.34	6.00E-17	1.33	8.22E-06	0.75395	189	0.001155
24	4.38	1.14E-17	4.10	7.28E-06	0.77144	184.5	0.001793
25	4.43	4.43E-18	3.91	7.85E-06	0.76131	185.3	0.0022
26	4.45	3.43E-18	4.18	7.67E-06	0.76348	188.3	0.001441
27	4.39	5.30E-18	6.78	6.92E-06	0.78126	188.6	0.000678
28	4.51	2.00E-17	7.60	6.76E-06	0.78614	202.9	0.000664
29	4.59	3.19E-17	7.37	7.06E-06	0.78217	221.8	0.000697
30	4.65	5.50E-17	6.86	7.09E-06	0.78428	240.4	0.000657
31	4.69	6.30E-17	7.52	7.51E-06	0.78517	251.4	0.000988
32	4.72	8.44E-17	3.25	1.02E-05	0.74775	273.3	0.000346
33	4.75	6.10E-17	2.55	1.02E-05	0.75087	461.2	0.000456
34	4.79	6.02E-17	5.98	8.89E-06	0.77886	351.1	0.001297
35	4.82	4.08E-17	7.00	8.93E-06	0.77763	342.2	0.001546
36	4.83	1.60E-17	7.43	9.23E-06	0.77115	316	0.001445
37	4.86	1.07E-17	10.42	8.10E-06	0.79203	300.6	0.003355
38	4.9	1.10E-17	8.82	8.66E-06	0.78524	304.4	0.002919
39	4.99	4.02E-18	6.15	1.04E-05	0.76183	319.7	0.001678

in the Fe^{2+}/Fe^{3+} redox couple. This phenomenon is also observed in the Mn and Co transformation region.

4. Conclusions

$LiCo_{1/3}Mn_{1/3}Fe_{1/3}PO_4$ has been successfully synthesized by a solid-state method and its crystal structure belongs to the olivine-type system. Due to the contribution of the Mn^{2+}/Mn^{3+} and Co^{2+}/Co^{3+} redox couples, $LiCo_{1/3}Mn_{1/3}Fe_{1/3}PO_4$ shows a high capacity of 140 mAh g^{-1} and working voltage of 3.72 V at a 0.05 C discharge rate. In-situ XRD experiments shows that $LiCo_{1/3}Mn_{1/3}Fe_{1/3}PO_4$ still maintains a stable structure at 5 V during charge/discharge. Although $LiCo_{1/3}Mn_{1/3}Fe_{1/3}PO_4$ is a solid solution of $LiCoPO_4$, $LiMnPO_4$ and $LiFePO_4$, the transition metals have different chemical activities. The diffusivity of lithium ion in the Fe^{2+}/Fe^{3+} and Mn^{2+}/Mn^{3+} regions is about 10^{-15} $cm^2\ s^{-1}$ but in the Co^{2+}/Co^{3+} region is only 10^{-16} $cm^2\ s^{-1}$. These results show that the contribution to the total capacity of the Co^{2+}/Co^{3+} redox couple is less than that of Mn^{2+}/Mn^{3+} and Fe^{2+}/Fe^{3+} redox couples.

Acknowledgments

The authors gratefully acknowledge the support of this work by the National Science Council of the Republic of China under the contract of NSC95-2221-E007-042. The authors would also like to thank W.T. Chuang for their technical assistance and the National Synchrotron Radiation Research Center (NSRRC) for use of X-ray diffraction facilities.

References

[1] A.K. Padhi, K.S. Nanjundaswamy, J.B. Goodenough, J. Electrochem. Soc. 144 (1997) 1188–1194.
[2] A. Yamada, S.C. Chung, K. Hinokuma, J. Electrochem. Soc. 148 (2001) A224–A229.
[3] A. Deb, U. Bergmann, E.J. Cairns, S.P. Cramer, J. Phys. Chem. B 108 (2004) 7046–7051.
[4] K. Zaghib, P. Charest, A. Guerfi, J. Shim, M. Perrier, K. Striebel, J. Power Sources 146 (2005) 380–385.
[5] H. Huang, S. Yin, L.F. Nazar, Electrochem. Solid-State Lett. 4 (2001) A170–A172.
[6] Z. Chen, J.R. Dahn, J. Electrochem. Soc. 149 (2002) A1184–A1189.
[7] S. Yang, Y. Song, P. Zavalij, M. Whittingham, Electrochem. Commun. 4 (2002) 239–244.
[8] S.T. Myung, S. Komaba, R. Takagai, N. Kumagai, Y.S. Lee, Chem. Lett. 7 (2003) 566–567.
[9] S.Y. Chung, J.T. Bloking, Y.M. Chiang, Nat. Mater. 2 (2002) 123–128.
[10] D.H. Kim, J. Kim, Electrochem. Solid-State Lett. 9 (2006) A439–A442.
[11] C. Delacourt, P. Poizot, S. Levasseur, C. Masquelier, Electrochem. Solid-State Lett. 9 (2006) A352–A355.
[12] F. Zhou, M. Cococcioni, K. Kang, G. Ceder, Electrochem. Commun. 6 (2004) 1144–1148.
[13] A. Yamada, Y. Takei, H. Koizumi, N. Sonoyama, R. Kanno, Chem. Mater. 18 (2006) 804–813.
[14] H.T. Kuo, T.S. Chan, N.C. Bagkar, G.Q. Liu, R.S. Liu, C.H. Shen, D.S. Shy, X.K. Xing, J.M. Chen, J. Phys. Chem. B 112 (2008) 8017–8023.
[15] X.J. Wang, X.Q. Yu, H. Li, X.Q. Yang, J. Mcbreen, X.J. Huang, Electrochem. Commun. 10 (2008) 1347–1350.
[16] J. Wolfenstine, J. Allen, J. Power Sources 136 (2004) 150–153.
[17] X.Q. Yang, J. McBreen, W.S. Yoon, C.P. Grey, Electrochem. Commun. 4 (2002) 649–654.
[18] P.Y. Liao, J.D. Duh, J.F. Lee, H.S. Sheu, Electrochim. Acta 53 (2007) 1850–1857.
[19] H.H. Chang, C.C. Chang, H.C. Wu, M.H. Yang, H.S. Sheu, N.L. Wu, Electrochem. Commun. 10 (2008) 335–339.
[20] Y.C. Chen, J.M. Chen, C.H. Hsu, J.W. Yeh, J.C. Shih, Y.S. Chang, H.S. Sheu, J. Power Sources 189 (2009) 790–793.

[21] Y.C. Chen, J.M. Chen, C.H. Hsu, J.F. Lee, J.W. Yeh, H.C. Shih, Solid State Ionics 180 (2009) 1215–1219.
[22] J. Chen, M.J. Vacchio, S. Wang, N. Chernova, P.Y. Zavalij, M.S. Whittingham, Solid State Ionics 178 (2008) 1676–1693.
[23] L. Laffont, C. Delacourt, P. Gibot, M.Y. Wu, P. Kooyman, C. Masquelier, J.M. Tarascon, Chem. Mater. 18 (2006) 5520–5529.
[24] G.Y. Chen, X.Y. Song, T.J. Richardson, Electrochem. Solid-State Lett. 9 (2006) A295–A298.
[25] A.K. Padhi, K.S. Nanjundaswamy, C. Masquelier, S. Okada, J.B. Goodenough, J. Electrochem. Soc. 144 (1997) 1609–1613.
[26] M. Yonemura, A. Yamada, Y. Takei, N. Sonoyama, R. Kanno, J. Electrochem. Soc. 151 (2004) A1352–A1356.
[27] P.P. Prosini, M. Lisi, D. Zane, M. Pasquali, Solid State Ionics 148 (2002) 45–51.
[28] F. Gao, Z. Tang, Electrochim. Acta 53 (2008) 5071–5075.